pubs.acs.org/Biomac

Article

Regiospecific Cellulose Orientation and Anisotropic Mechanical Property in Plant Cell Walls

Jongcheol Lee, Juseok Choi, Luyi Feng, Jingyi Yu, Yunzhen Zheng, Qian Zhang, Yen-Ting Lin, Saroj Sah, Ying Gu, Sulin Zhang, Daniel J. Cosgrove, and Seong H. Kim*

Cite This: *Biomacromolecules* 2023, 24, 4759−4770

Read Online

ACCESS | Metrics & More | Article Recommendations | Supporting Information

ABSTRACT: Cellulose microfibrils (CMFs) are a major load-bearing component in plant cell walls. Thus, their structures have been studied extensively with spectroscopic and microscopic characterization methods, but the findings from these two approaches were inconsistent, which hampers the mechanistic understanding of cell wall mechanics. Here, we report the regiospecific assembly of CMFs in the periclinal wall of plant epidermal cells. Using sum frequency generation spectroscopic imaging, we found that CMFs are highly aligned in the cell edge region where two cells form a junction, whereas they are mostly isotropic on average throughout the wall thickness in the flat face region of the epidermal cell. This subcellular-level heterogeneity in the CMF alignment provided a new perspective on tissue-level anisotropy in the tensile modulus of cell wall materials. This finding also has resolved a previous contradiction between the spectroscopic and microscopic imaging studies, which paves a foundation for better understanding of the cell wall architecture, especially structure−geometry relationships.

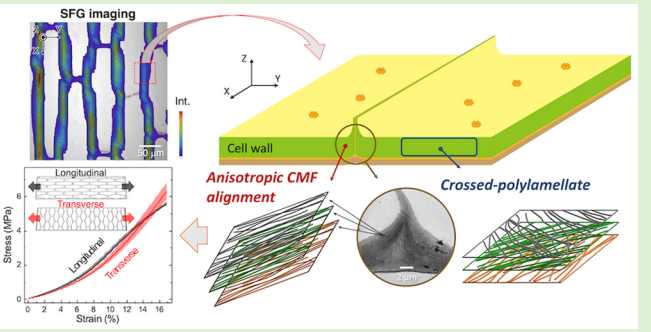

INTRODUCTION

Although the composition and structure of individual plant cell walls vary depending on their functions,[1−4] it is generally accepted that cellulose microfibrils (CMFs) are the major load-bearing component that governs the tensile mechanical properties of the cell wall.[5] Each elemental CMF consists of 18 linear chains of β-1,4-linked glucose units synthesized from cellulose synthase complexes (CSCs).[6,7] The cellulose chains are assembled through hydrogen-bonding interactions side by side into sheets and through van der Waals interactions between sheets, forming a crystalline microfibril.[8−10] The mesoscale structural assemblies of these nanocrystalline CMFs with other polysaccharides in cell walls must be optimized to confer specific biological and physical properties at cellular or tissue levels that are harmonized for the survival and growth of the entire plant.[1,2,11]

The CMFs in cell walls play an important role in controlling various aspects of plant growth such as cell size and anisotropic cell expansion,[3,12,13] and the relationship between cellulose structure and wall mechanical properties requires accurately knowing the organization of CMFs within the cell wall. For this purpose, onion epidermal walls are considered a good model system for such studies because they are easy to prepare for characterization and mechanical testing.[14−18] The outermost periclinal wall of the onion epidermis can be easily peeled off, revealing the most recently deposited CMFs on the cytoplasm side of the wall.[19,20] Previously, these CMFs were imaged with atomic force microscopy (AFM) and field emission scanning electron microscopy (FESEM), which revealed a crossed-polylamellate structure of CMFs.[18,21−23] In each lamella, CMFs are loosely aligned along a preferential orientation, which varies by 30−90° among the adjacent lamellae.[18] Such variations in the dominant CMF orientations between the neighboring lamellae could result in an equal probability of all orientations when averaged over all lamellae inside the wall. A recent study using cryoelectron tomography reported a bimodal distribution of microfibrils along 42 ± 8° and 135 ± 10° with respect to the longitudinal axis of the cell.[24]

In contrast, infrared spectroscopic studies suggested a different picture, namely, "anisotropic" orientational distribution. Most spectroscopic analyses of large-area samples have suggested that CMFs in the onion epidermis have a slightly anisotropic orientation with a preferential axis tilted toward the transverse direction of the cell.[15,16,25] This anisotropic distribution of CMFs has been thought to be the origin of the larger mechanical extensibility of epidermal walls along the longitudinal direction than the transverse direction.[26,27]

Received: May 30, 2023
Revised: August 12, 2023
Published: September 13, 2023

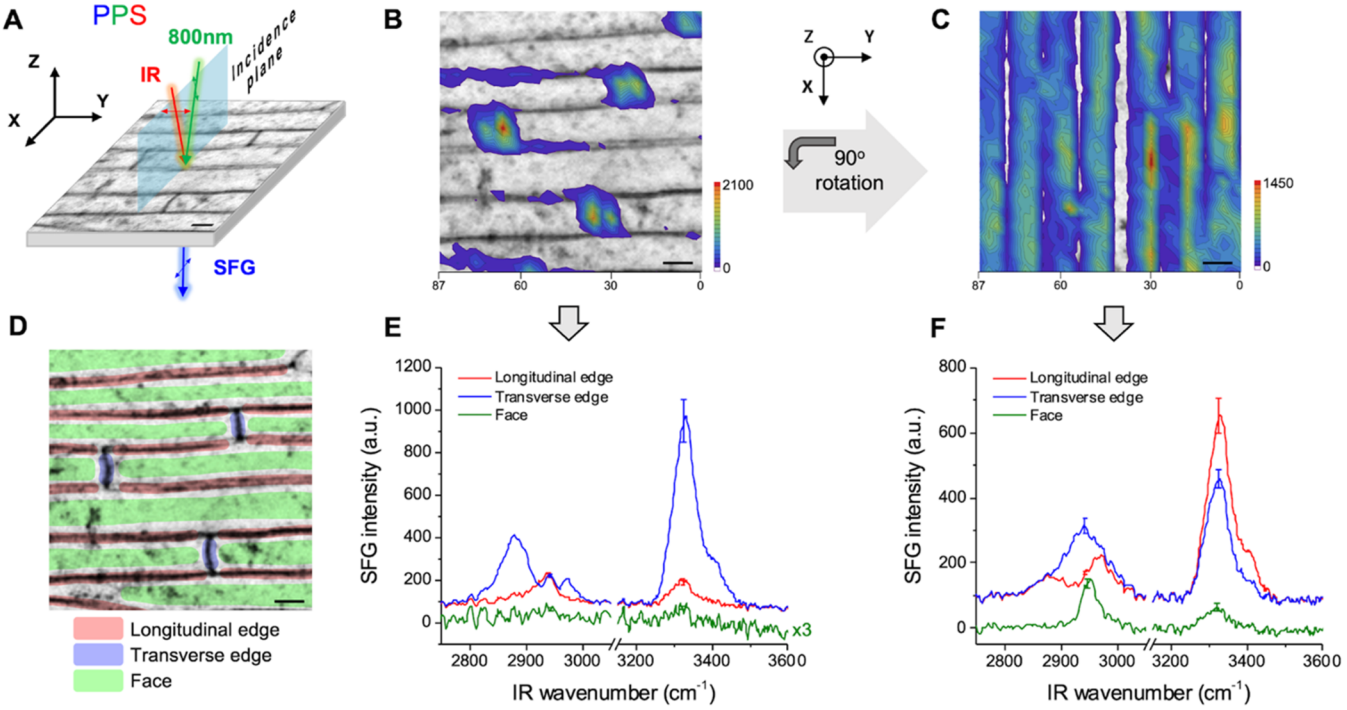

Figure 1. Microscopic SFG analysis of the *Arabidopsis* stem epidermal cell wall. (A) Microscopic pps-SFG analysis (90 μm × 90 μm) of an *Arabidopsis* stem epidermal peel hydrated in D_2O. The aspect ratio of cells is 17 ± 3. The sample is lying in the *XY* plane, and the laser incidence is in the *XZ* plane. The polarizations of the probe beams are p for SFG, p for 800 nm, and s for IR. (B, C) Hyperspectral images of the 3320 cm^{-1} SFG signal superimposed on the optical image. (D) Regions from which full spectra are extracted. (E, F) SFG spectra averaged over the longitudinal and transverse edge regions and the face regions. The error bar is the standard error of mean at ~2944 and ~3320 cm^{-1}. The scale bars are 10 μm. The data shown in panels (B, E) and (C, F) are when the long axis of the cell is perpendicular and parallel to the laser incidence plane, respectively. In panels (B, C), note that the lowest intensity area in the contour plots was adjusted to be transparent to show the underlying optical images. Similar features are observed in two additional data sets (Figure S1).

However, these results are inconsistent with the crossed-polylamellate structure in which the averaged CMF orientations across the wall thickness are expected to be nearly isotropic[16,18,25] or diagonally bimodal.[24] Studies of onion epidermis stained with Congo Red and analyzed by polarization confocal microscopy reported the net cellulose orientation varying from transverse to random to longitudinal depending on the growth stage of the scale but generally running perpendicular to the major growth direction.[17,28]

In this study, we have used vibrational sum frequency generation (SFG) microscopy to reassess the cellulose orientation in the epidermal wall in greater detail. SFG is known to selectively detect crystalline cellulose in plant cell walls, and its spectral features are sensitive to the nano-to-mesoscale structural orders of cellulose.[9,29−31] Through subcellular scale imaging, the "face" and "edge" regions of cells in the epidermal peel could be distinguished.[32,33] Here, the edge is defined as the region where the anticlinal wall touches the periclinal wall during cell division and eventually becomes the junction of two fully developed cells. In other words, the edge region is where two cells meet in the periclinal wall plane or in the peeled epidermis. The face is the flat and uniform-thickness region in the periclinal wall plane surrounded by the edge regions in the peeled epidermis. The hyperspectral SFG imaging of epidermal walls of *Arabidopsis* stem, maize coleoptile, and onion scales showed that the microfibrils in the edge region are preferentially aligned perpendicular to the plane of anticlinal walls. Finite element analysis (FEA) of a rectangular cell shape predicted that the turgor pressure of the cell generates tensile stress in the edge region parallel to the preferential CMF orientation, which might suggest that the anisotropic CMF orientation distribution in the edge region originates from the anisotropic stress distribution and directions.[12,34−36] Furthermore, FEA with the nonuniform CMF assemblies provided a new perspective on the anisotropic tensile modulus of the onion epidermal wall.[37−39]

EXPERIMENTAL SECTION

Materials. Fresh white onion bulbs (*Allium cepa*, cv. Cometa) were purchased from a local grocery store. The fresh hydrated scale immediately appearing after the removal of the dried scales was numbered as first, and the outermost single layer of cell walls (abaxial epidermis) of the fifth scale was analyzed. *Arabidopsis thaliana* (ecotype Columbia-0) was obtained from the Arabidopsis Biological Resource Center (ABRC) at Ohio State University. The seed growth condition is described in the previous publication.[40] After 10 days, seedlings were transferred to pots containing soil and grown in a growth chamber (Percival, Perry, GA) at 22 °C under a 16 h light and 8 h dark cycle for 7 weeks. Hybrid maize seeds (Zea mays, 5480GENVT2PRIB) from SEEDWAY, LLC. (Hall, NY) were soaked in water for 30 min, sown on an absorbent paper cloth saturated with water, and placed in a plastic box wrapped in aluminum foil. Seeds were incubated in the dark at 28 °C for 4 days.

Preparation for SFG Analysis. The fifth-scale onion epidermis was peeled and rinsed with deionized water several times. The details of this protocol are described in previous publications.[16,19,20,41] The maize coleoptile epidermis was peeled approximately 0.5 cm from the tip. The *Arabidopsis* stem epidermis was peeled approximately 15 cm from the bottom using branches, and the single layer of cell wall at the end of the peel was cut and used. The excised and rinsed peels were immersed in D_2O with 0.02% sodium azide overnight. Subsequently, the peels were mounted on a slide glass with the plasma membrane side facing up.

https://doi.org/10.1021/acs.biomac.3c00538
Biomacromolecules 2023, 24, 4759−4770

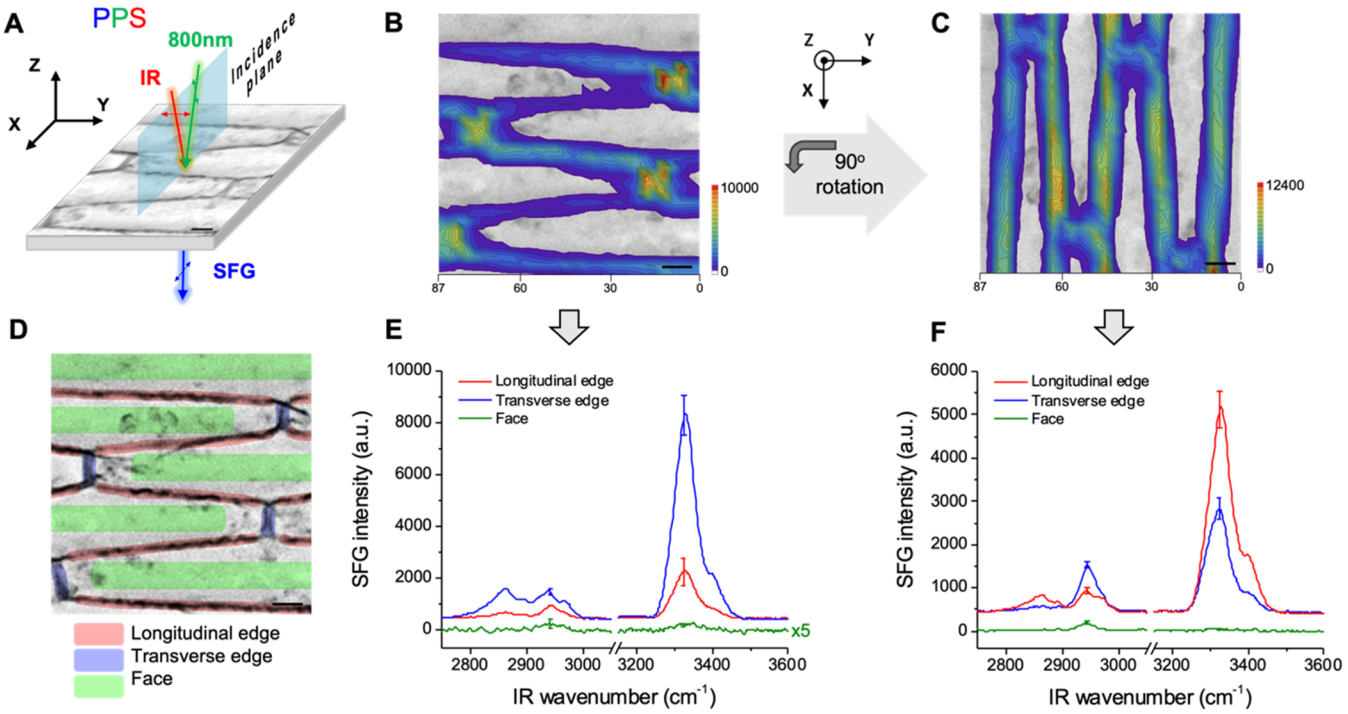

Figure 2. Microscopic SFG analysis of the maize coleoptile epidermal cell wall. (A) Microscopic pps-SFG analysis (90 μm × 90 μm) of a maize coleoptile epidermal peel hydrated in D_2O. The aspect ratio of cells is 16 ± 4. (B, C) Hyperspectral images of the 3320 cm^{-1} SFG signal superimposed on the optical image. (D) Regions from which full spectra are extracted. (E, F) SFG spectra averaged over the longitudinal and transverse edge regions and the face regions. The scale bars are 10 μm. The figure details are the same as in Figure 1. Similar features are observed in two additional data sets (Figure S2).

After a few drops of D_2O were applied, a coverslip was placed on the sample. After removing any overflowing liquid, the coverslip edges were sealed with nail polish to prevent sample dehydration.

Vibrational SFG Microscopy System. A broad-band SFG system with 800 nm pulses (pulse width ~85 fs with a 2 kHz repetition rate) was utilized for this experiment. A detailed description of the microscopic SFG system can be found in previous publications.[42,43] Briefly, our custom-built SFG microscopy system delivers the 800 nm and broad-band, tunable IR pulses colinearly but spatially separated. After the two beams pass the aperture of a reflective objective, the primary convex mirror reflects them to the opposite sides and the secondary concave mirror focuses them onto samples from the opposite sides. For the analysis of the onion epidermis, areas of 300 μm × 300 μm were scanned with a 10 μm step distance and a 1 s acquisition time, using a 15× reflective objective, which produced a Gaussian-like beam shape with ~5.4 μm along the *X*-axis, ~7.9 μm along the *Y*-axis, and ~26 μm along the *Z*-axis in the lab coordinate (see Figure 1).[42] For the analysis of the maize coleoptile epidermis and *Arabidopsis* stem epidermis, areas of 90 μm × 90 μm were scanned with a 3 μm step distance and a 1 s acquisition time, using a 36× reflective objective, which generated a Gaussian-like beam shape with ~2.4 μm along the *X*-axis, ~4.1 μm along the *Y*-axis, and ~15 μm along the *Z*-axis.[42] Note that this dimension is based on the one-sigma standard deviation of the Gaussian beam shape; the tail of the beam spread much larger than this dimension. The same 36× objective and settings were used for the analysis of the cross-sectioned onion epidermis, and the scan area varied depending on the sample size (see Figure S4). The SFG spectra of fully hydrated samples in D_2O were collected at two different sample mount geometries (0 and 90° with respect to the laser incidence plane) to study the preferential orientation of CMFs. The hydration with D_2O instead of H_2O was to avoid the attenuation of the IR probe beam in the OH stretch band region. The polarization combination used for data collection was p for the SFG signal, p for 800 nm, and s for IR (which will be called pps hereafter). The effect of CMF orientation on SFG intensities of cellulose-characteristic peaks was simulated using the theoretical algorithm fully described in the previous publication.[44]

Field Emission Scanning Electron Microscope (FESEM). The onion fifth-scale abaxial epidermal strips from the middle of the convex surface were treated with pectate lyase to remove the pectin. Then, the samples underwent critical point drying through a Leica EM CPD 300, and the inner side (plasma membrane side) of the epidermis was imaged by a Zeiss Sigma FESEM. The detailed experimental procedure is described in previous publications.[18,45] The analysis of the microfibril orientation distribution in the Supporting Information was conducted using OrientationJ.[46]

Transmission Electron Microscope (TEM). The epidermal cell walls including several cells in the onion fifth scale were shaved off without peeling and underwent a high-pressure freezing through (Leica, Wetzlar, Germany) an EM HPM 100 and media substitution through a Leica automatic freeze substitution (AFS). The tissue blocks were trimmed, and the cross section was imaged by an FEI Tecnai Spirit G2 TEM (FEI, USA). The detailed procedure was described in the previous publications.[18]

Finite Element Analysis (FEA). The FEA simulations were conducted with Abaqus CAE (Dassault Systèmes, Simulia Corporation). For the stress distribution simulation, a 75 mm (width) × 45 mm (height) × 200 mm (length) rectangular prism was generated, and the inside of the prism was cut out leaving the top and side wall thicknesses of 1 mm and a bottom thickness of 7 mm, mimicking the epidermal cells.[47] The corners were rounded with a radius of 3 mm. The outer surface of the top face was fixed, and the periodic boundary condition was applied to the lateral faces, assuming that they were counterbalanced and not deformable by the neighboring cells. The bottom face was allowed to deform. An isotropic homogeneous elastic modulus of 350 MPa for the material[39] and a load of 0.6 MPa for the pressure inside[48,49] were applied in the model.

For the tensile modulus simulation, a two-dimensional repetitive volume element (RVE) was modeled with the idealized cell shape; the parameters used for RVE were based on the previous study by Shafayet Zamil et al. (120 μm long, 30 and 60 μm short and wide width).[39] The width of the cell edge region was set to 10 μm. The elastic and isotropic moduli of the face wall area were assumed to be 15 MPa.[5] For the edge

https://doi.org/10.1021/acs.biomac.3c00538
Biomacromolecules 2023, 24, 4759−4770

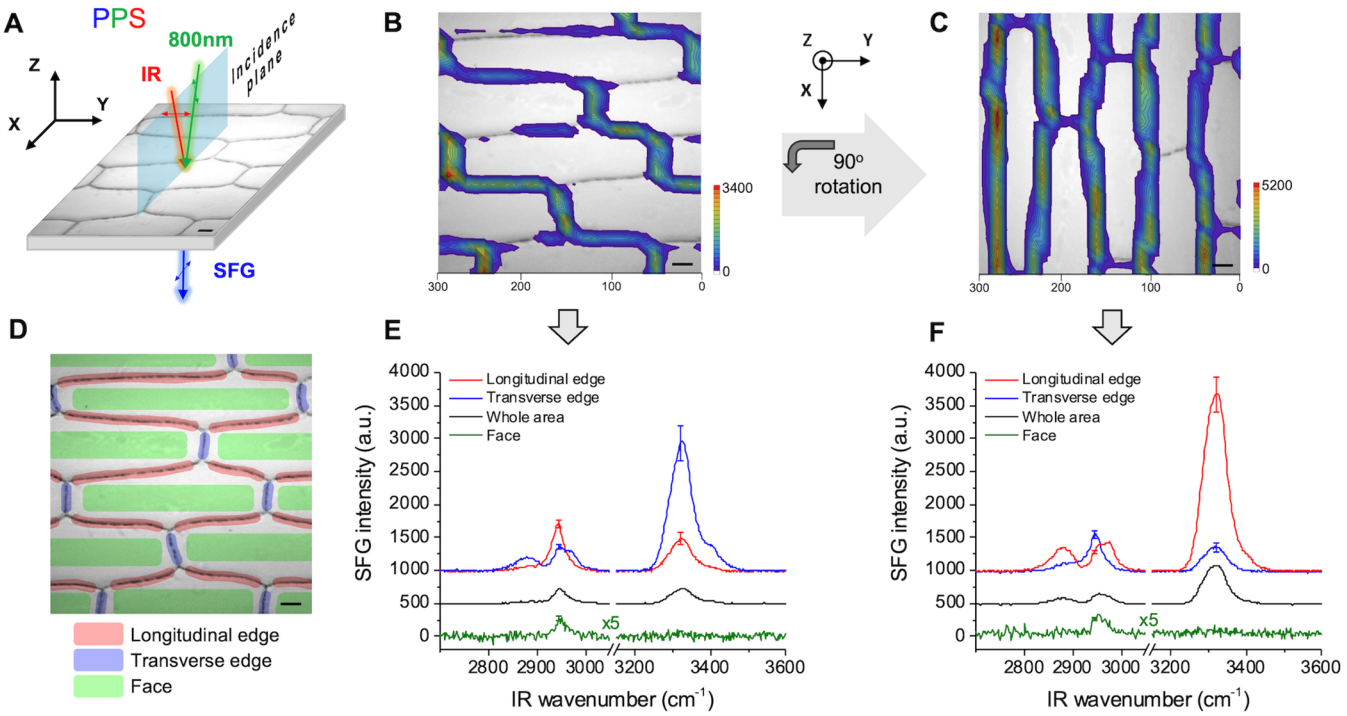

Figure 3. Microscopic SFG analysis of the onion epidermal cell wall. (A) Microscopic SFG analysis (300 μm × 300 μm) of an abaxial epidermis of the fifth-scale onion hydrated in D_2O. The aspect ratio of cells is 3.6 ± 0.2. (B, C) Hyperspectral images of the 3320 cm^{-1} SFG signal superimposed on the optical image. (D) Regions from which full spectra are extracted. (E, F) SFG spectra averaged over the longitudinal and transverse edge regions and the face regions. Panels (E, F) also show the averaged SFG spectra of the whole area of panels (B, C). The scale bars are 20 μm. The figure details are the same as in Figure 1. Similar features are observed in two additional data sets (Figure S3).

regions, various values of orthotropic and elastic "effective" moduli were assumed, and the tissue-level longitudinal and transverse moduli were calculated with the periodic boundary condition.[50] Poisson's ratio of 0.48, which is a typical value for incompressible biological materials, was used for the face region for the stability criterion and to reduce the convergence issue in Abaqus CAE.[39] The same Poisson's ratio and shear modulus in the face region were assumed for the edge region.

Tensile Testing of Onion Epidermal Walls. Onion abaxial epidermal wall strips (10 mm × 3 mm × 7 μm) were peeled from the center region of the fifth scale of onion bulbs. Wall strips peeled from longitudinal (along the long axis of onion cells) and transverse directions were stretched at a speed of 5 mm/min on a custom-built stretching device where the position of the clamp and applied loading were recorded simultaneously.[20] The extensometer and stretch experiment procedure were described in the previous publications.[5,22] The stress was calculated by dividing the applied force by the initial cross-sectional area of the wall strip (3 mm × 7 μm). The strain was the amount of extension divided by the initial gauge length of 5 mm. Modulus was calculated as the slope from 0 to 3% strain by linear regression (n = 11 and 9 for the longitudinal and transverse directions, respectively).

Cross-Polarized (CP) Optical Microscopy. The cross-polarized (CP) optical microscopic imaging of the onion epidermis was carried out with an Olympus BX61 compound microscope equipped with a UPLFL 10× objective (NA = 0.3), a polarizer, and a U-AN360 analyzer. Images at different sample orientations were captured with a fixed exposure time under identical conditions.

RESULTS AND DISCUSSION

SFG Imaging of CMF with Subcellular Resolution. Figures 1−3 show the hyperspectral SFG images and full spectra of three different regions in *Arabidopsis* stem, maize coleoptile, and fifth-scale onion epidermis (see also Figures S1−S3 for data from replicas). While there are slight differences among the replica and across the three plants, there are common features observed in hyperspectral images of these epidermal walls. In the face region, the cellulose-characteristic CH stretch peak can be identified around 2944 cm^{-1}, and it does not change upon the rotation of the sample by 90° (Figures 2 and 3F). Also, the CH intensity is very weak and the 3320 cm^{-1} OH stretch peak, characteristic of cellulose, is barely identifiable above the noise level. In the case of epidermal cell walls of *Arabidopsis* stem (Figure 1F), the OH signal intensity in the face region appeared stronger than those in the maize coleoptile and onion epidermis (Figures 2 and 3F) and there is a 2944 cm^{-1} intensity change upon the sample rotation. However, this is likely caused by the contribution from the edge region because the tail of the Gaussian laser beam from the 36× objective in the Y-axis is spread over the transverse width of the epidermal cells of *Arabidopsis* stem.

In contrast, in the edge region, the SFG intensity is much stronger than in the face region (Figures S1−S4) and the 3320/2944 cm^{-1} intensity ratio varies upon the rotation of the sample by 90°. The ratio is larger when the edge lines (dark lines in the optical image) are parallel to the pps laser incidence plane, and it is smaller when the edge lines are perpendicular to the laser incidence plane. The SFG hyperspectral images at 3320 cm^{-1} (Figure 1B,C) show the intensity enhancement and reduction in the two different edge regions upon the sample rotation; the transverse edge regions have a higher intensity than the longitudinal in Figure 1B, and this trend switches in Figure 1C. Moreover, within the CH stretch region, the 2860−2880/2944 cm^{-1} and 2968/2944 cm^{-1} intensity ratios also vary upon the rotation of the sample by 90°, which is similar to the 3320/2944 cm^{-1} ratio trend as observed in previous studies with aligned cellulose microfibrils in natural plant cell walls.[44,51,52]

https://doi.org/10.1021/acs.biomac.3c00538
Biomacromolecules 2023, 24, 4759−4770

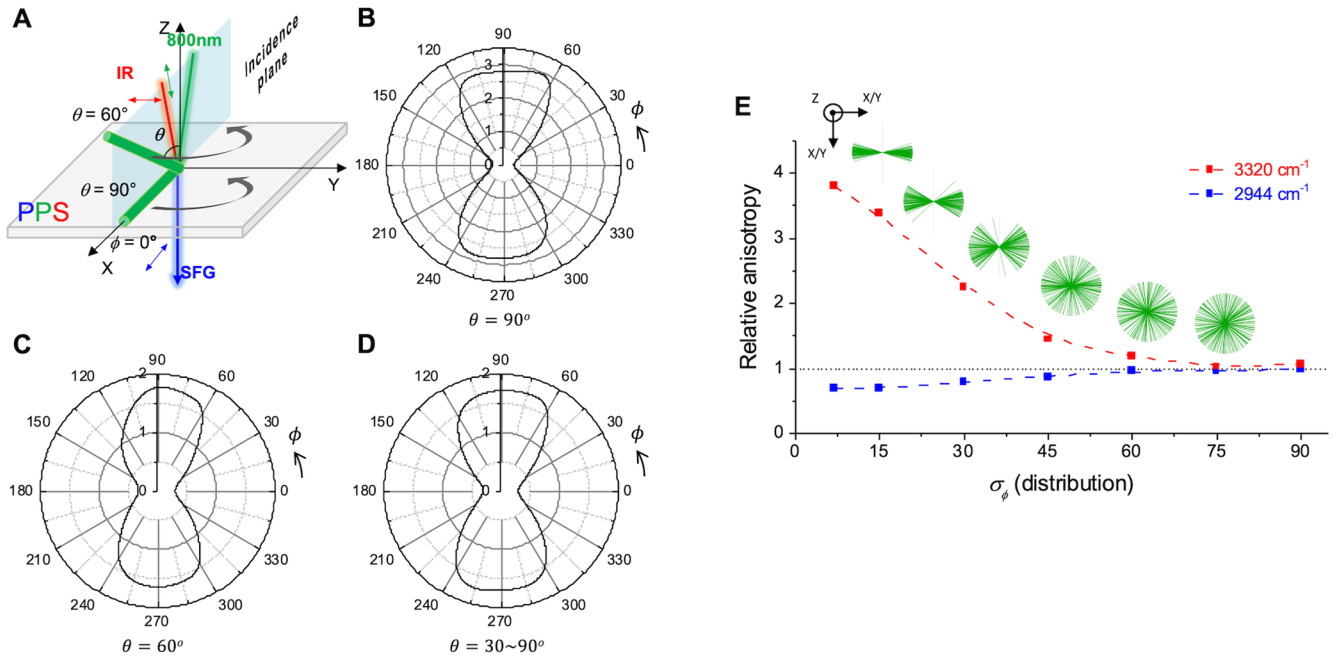

Figure 4. Theoretically calculated azimuth angle-dependent pps-SFG intensities with tilt angles considering the curved walls in the edge region. (A) Schematic of a cellulose crystal at two different tilt angles: $\boldsymbol{\theta}$ = 60 and 90°. (B–D) Azimuth angle ($\boldsymbol{\phi}$) dependent pps-SFG intensity ratio of 3320 and 2944 cm^{-1} peaks (OH/CH) at different tilt angles: $\boldsymbol{\theta}$ = 90° (B), 60° (C), and the average 30–90° (D). In the calculation, the microfibril angle distribution in the azimuthal plane (σ_ϕ) was assumed to be 15°. The average of $\boldsymbol{\theta}$ = 30–90° represents the curved microfibrils in the edge region cell wall based on the TEM images in Figure 7. (E) Azimuth angle distribution (σ_ϕ)-dependent relative anisotropy of 3320 and 2944 cm^{-1} peaks in their polar plots; the relative anisotropy is defined as the averaged SFG intensity when $\boldsymbol{\phi}$ = ~90° divided by that of $\boldsymbol{\phi}$ = ~0°. The azimuth angle distribution (σ_ϕ) is the degree of distribution of microfibrils in the azimuthal plane. The insets show 100 lines generated based on N[0/90°, σ_ϕ] (σ_ϕ = 7, 15, 30, 45, 60, 75, 90°), which represents the degree of angle distribution of CMFs in the *XY* plane. The data shown here are the average of the calculation results simulated with $\boldsymbol{\theta}$ = 90–30° with a 15° interval. In the calculation, the local deviation of CMF polarity from bidirectionality (i.e., unidirectional bias) was allowed, although the overall polarity of CMFs in the entire system is unbiased. In the calculation, the inter-CMF distance, as well as the CMF diameter, was chosen to match the volumetric concentration of CMFs in the fully hydrated epidermal walls of onion.[18,22]

For the stronger SFG intensity in the edge region as compared to that of the face region in Figures 1–3 and S1–S3, one could speculate if this is because the edge region is thicker than the face region. This possibility was tested and ruled out by analyzing the cross-sectional samples placed vertically. In this geometry, the sample thickness along the *Z*-axis was constant. Since all three plants (Figures 1–3) show similar trends in terms of the difference in SFG spectral features between the edge and face regions, and onion epidermis is easier to prepare, we have chosen onion epidermis for this cross-sectional study. In Figure S4, the SFG spectra in the edge region showed a consistent feature shown in Figure 3 and the 2944 cm^{-1} peak intensity is about 3–4 times larger than in the face region. If the entire CH band area is considered, the difference is even larger. Also, the face region exhibits a negligible OH stretch intensity, while the edge region gives a strong signal in the OH stretch region.

It should be noted that the contribution of the residual anticlinal wall above the edge regions was also negligible. In Figure S5, the anticlinal wall is so thin that the fragments attached to the edge region bend over onto the periclinal wall plane.[47] In the cross-polarization micrograph (Figure S5B), anticlinal wall fragment regions still look dark, suggesting that the cellulose amount added by the anticlinal wall is insignificant. Also, the SFG intensities in these regions (marked in Figure S5A) are not higher than in the other regions without such fragments in the face region in Figure 3. Thus, the reason that the SFG intensity of the edge regions in Figures 1–3 and S1–S3 is stronger cannot be due to the presence of anticlinal wall fragments.

Anisotropic Alignment of CMFs in Edge Regions. In previous SFG analyses of uniaxially aligned cellulose nanocrystals (CNCs) and highly aligned CMFs in the G-layers of reaction woods and ramie fibers,[51,53] similar changes in the relative intensities of 2860–2880, 2968, and 3320 cm^{-1} peaks with respect to the 2944 cm^{-1} peak were observed upon a 90° rotation of the sample. In theoretical calculations of the SFG intensity of cellulose, it has been shown that when the cellulose chain axis of CNCs and CMFs is aligned with the electric field of the IR beam (i.e., the third letter in the polarization combination), the 3320 cm^{-1} OH intensity is enhanced and the 2944 cm^{-1} CH intensity is relatively weak.[44] This means that, in the pps-SFG spectrum, the 3320/2944 cm^{-1} intensity ratio will be high when the CMF axis is aligned perpendicular to the laser incidence plane. In contrast, when CMFs are aligned parallel to the laser incidence plane, this intensity ratio becomes smaller as compared to its orthogonal orientation case. The relative intensities of the 2860–2880 and 2968 cm^{-1} peaks with respect to that of the 2944 cm^{-1} peak will show a similar trend for the highly anisotropic distribution case.[44]

When this knowledge is employed to interpret the data in Figures 1–3 and S1–S3, it is found that CMFs in the edge region of the outermost periclinal wall are anisotropically aligned with the dominant axis perpendicular to the plane of the anticlinal walls. This interpretation does not change even if the lamellae are gradually tilted out of the periclinal plane (Figure 4B–D). In the edge region, the lamellae (in which CMFs are laid) gradually deviate out of the periclinal wall plane (*XY* plane in Figures 1–4A) and transition into the anticlinal wall (*XZ* or

https://doi.org/10.1021/acs.biomac.3c00538
Biomacromolecules 2023, 24, 4759–4770

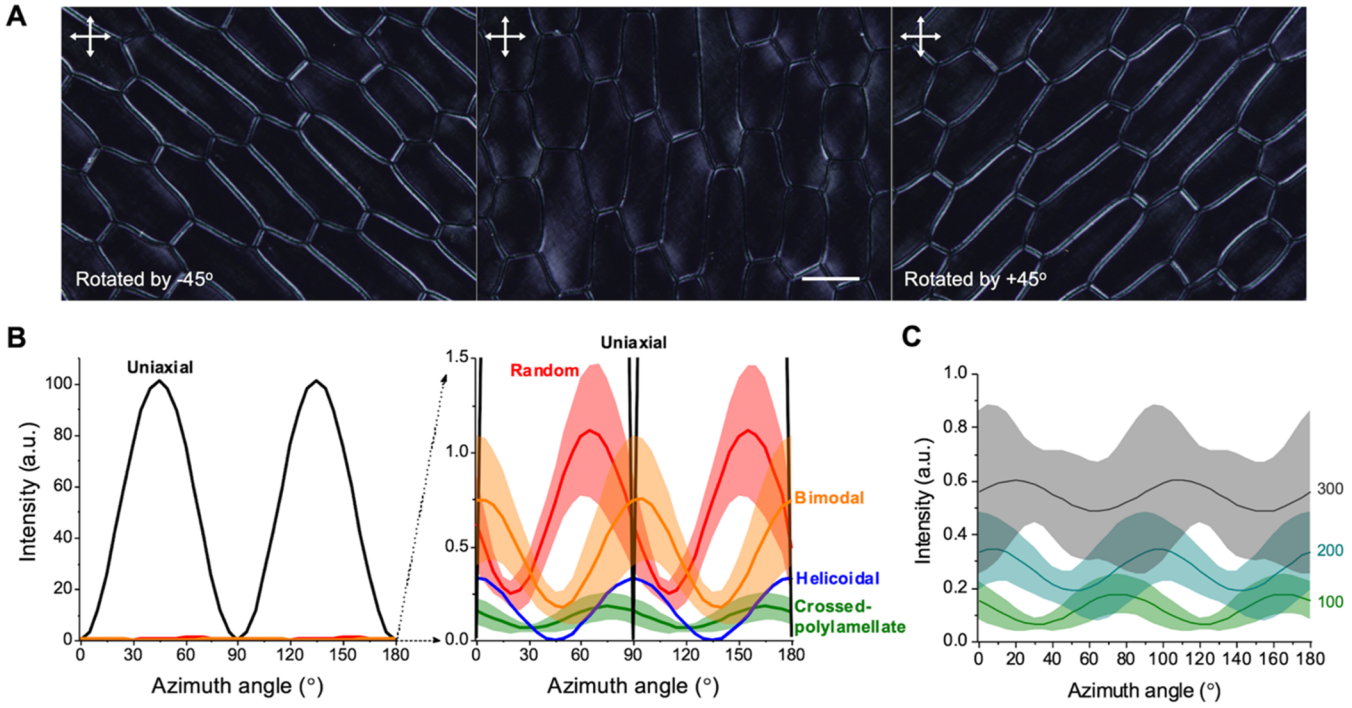

Figure 5. Cross-polarization (CP) microscopy analysis. (A) CP optical images of the abaxial epidermal wall of the fifth scale of onion at three different sample orientations with respect to the polarizer axis. The scale bar is 100 μm, and the white arrows show the polarizer axes. (B) Calculated azimuth angle dependence of CP transmittance for five different organizations of 100 cellulose crystals along the light propagation axis: nearly uniaxial (σ_ϕ = 10°), helicoidal (with $\Delta\phi$ = +10°), crossed-polylamellate ($\Delta\phi$ = 61.9° ± 16.4° SD), bimodal (ϕ = 42° ± 8° and 135° ± 10°), and completely random within the plane perpendicular to the light propagation axis.[18,24] (C) Calculated azimuth angle dependence of the CP transmittance of 100, 200, and 300 cellulose crystals with the crossed-polylamellate organization. The average (solid line) and standard error (shaded area) of 10 simulation results are shown.

YZ plane). To study the effect of the tilt angle, the theoretical SFG intensity ratios of 3320 and 2944 cm^{-1} are calculated in Figure 4B−D using the numerical simulation algorithm developed recently.[44] The azimuth angle-dependent polar plots show that the difference is small as the tilt angle (θ) changes between 30° and 90°. The azimuth angle dependence of the 3320/2944 cm^{-1} ratio (Figure 4B−D) is also in good agreement with the experimental data in Figures 1−3 and S1−S3. In Figures 1−3B, the CMFs in the longitudinal edge region (red in Figures 1−3E) are parallel to the laser incidence plane (ϕ = 0°) and the 3320 cm^{-1} intensity is lower than the 2944 cm^{-1} intensity. In contrast, the CMFs in the transverse edge region (blue in Figures 1−3E) are perpendicular to the laser incidence plane (ϕ = 90°) and the 3320 cm^{-1} intensity is higher than the 2944 cm^{-1} intensity. In Figures 1−3C, when the sample is rotated by 90°, those azimuth angles of preferentially aligned CMFs in the two edge regions are switched and the trend of the SFG intensities of 3320 and 2944 cm^{-1} is also switched.

Furthermore, we have studied the effect of the degree of orientational anisotropy on the azimuth angle-dependent polar plot through the simulation. Figure 4E shows the relative anisotropy (the ratio of the intensity at ϕ = ~90 and ~0°) in the 2944 and 3320 cm^{-1} polar plots as a function of the distribution of microfibrils (σ_ϕ). When the microfibrils have a large orientational distribution (i.e., $\sigma_\phi \geq$~75°, nearly isotropic), the SFG signal intensity has no dependence on the azimuth angle (ϕ) of the sample with respect to the laser incidence plane and the relative anisotropy is ~1. As the degree of CMF orientational anisotropy increases (i.e., σ_ϕ decreases), the pps-SFG intensity at 3320 cm^{-1} becomes much larger at ϕ = ~90° than at ϕ = ~0°; thus, the ϕ dependence becomes larger. In contrast, the pps-SFG intensity at 2944 cm^{-1} becomes slightly smaller at ϕ = ~90° than at ϕ = ~0° as the degree of anisotropy increases. From the experimental spectra in Figures 1−3 and S1−S3, it can be seen that the relative anisotropy is 0.5−1 for the 2944 cm^{-1} peak and 3−5 for the 3320 cm^{-1} peak in the longitudinal edge region. The transverse edge region shows similar trends. Comparing these values with the simulation results in Figure 4E suggests that the degree of anisotropic orientational distribution (σ_ϕ) of CMFs was around 30° or less from the dominant alignment direction. Even though the SFG calculation has proven to be valuable to study the orientation of CMFs, it has limitations in predicting accurate values in this study due to inherent assumptions and simplifications such as the isotropic Raman tensor.[44]

Cross-polarization (CP) optical imaging also supported the high degree of CMF alignment in the edge region. Figure 5A shows the CP optical micrographs of the abaxial epidermis of the fifth scale of onion. When the edge lines are ±45° with respect to the two crossed polarizer axes (two double-sided arrows), both sides of the anticlinal wall in the edge region are bright, while the face region is dark. When the edge lines are aligned with the polarizer axes, then the brightness contrast between the face and edge regions is reduced significantly. To interpret the CP micrographs in Figure 5A, we have theoretically calculated the transmittance of the linearly polarized light through a matrix containing 100 cellulose crystals packed with five different assemblies: (i) uniaxially aligned, (ii) random, (iii) crossed-polylamellate, (iv) helicoidal, and (v) bimodal. The details of the calculation are in Figure S6 and Supporting Information. Figure 5B shows that, when CMFs are highly uniaxially aligned and the preferential alignment axis is at 45 and 135° with respect to the

https://doi.org/10.1021/acs.biomac.3c00538
Biomacromolecules 2023, 24, 4759−4770

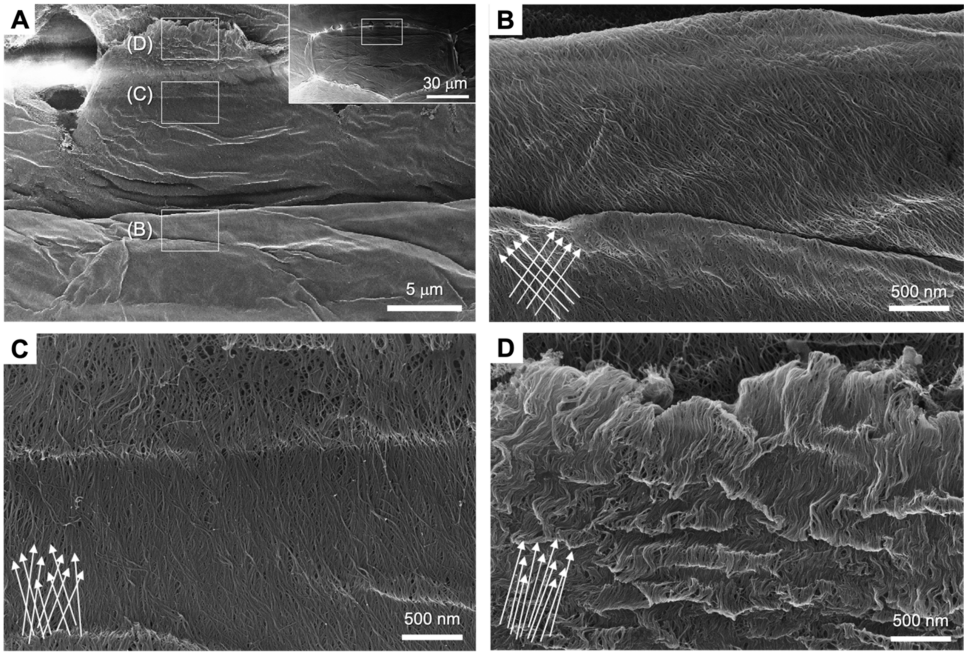

Figure 6. FESEM images of the onion epidermal cell wall. (A) Low-magnification image showing both the edge and face regions. The inset in panel (A) shows the entire cell, and the marked box is panel (A). Also shown are high-magnification images of the (B) face, (C) edge region, and (D) residual anticlinal wall of the epidermal cell wall. Arrows in the images represent the directions and distribution of microfibrils; the detailed analysis of the CMF distribution in panels (B, C) is in Figure S8. Note that wrinkles running across the entire image of each panel are due to the shrink and collapse of the cell wall during the sample drying. A similar trend was observed in three replicates (Figure S7A–L).

polarizer axes, the CP transmittance is about 2 orders of magnitude larger than the other four cases. Thus, the large azimuth angle-dependent intensity changes in the edge regions must be from the aligned microfibrils parallel/perpendicular to the edge lines. Additionally, the higher degree of birefringence associated with the cellulose crystal structure can be obtained when CMFs are highly aligned but not with a high concentration of randomly or isotropically oriented CMFs. Simply increasing the CMF concentration by a factor of 3 while keeping the cross-polylamellate structure (Figure 5C) could not increase the CP transmittance to the level found in the edge region. This CP-transmission result confirms the preferential alignment of CMFs in the edge region.

Additional supporting evidence for the anisotropic CMF distribution in the edge region can be found through the direct imaging of CMFs exposed in the cytoplasm side of the cell wall, although this approach reveals the distributions in the top two layers only (sometimes up to 3 layers).[18] Figure 6A displays a low-magnification FESEM image of the abaxial epidermal wall of the fifth scale of onion after pectin removal through pectate lyase treatment, and Figure 6B–D shows high-resolution images of CMFs in three distinct regions (see also Figure S7A–L). In the face region (Figure 6B), the crossed-polylamellate patterns of CMFs in the topmost and underneath lamellae can be seen clearly.[18] In the edge region (Figure 6C), the CMFs accessible by FESEM are relatively aligned toward the anticlinal wall direction (see Figure S8). This direction is consistent with the preferentially aligned CMFs found by the hyperspectral SFG analysis in the edge region. In the region that is believed to be the collapsed fragments of the anticlinal wall (Figure 6D), CMFs appear to be highly aligned toward the anticlinal wall direction.

Angular Distribution of CMFs in the Face Region. The absence of angular orientation dependence of the SFG spectral features in the face region is consistent with the nearly isotropic CMF orientation distribution expected from the crossed-polylamellate structure or the diagonally bimodal distribution.[18,24] This is also supported by the low transmission intensity of the face region in the CP imaging (Figure 5). The OH SFG intensity of CMFs in the face region is quite weak, while the CH signal is still measurable (Figures 1–3 and S1–S4). In the face region in primary cell walls, elementary fibrils are found as "singletons", and they often merge together, forming "bundles".[18,21,22] The elementary CMFs with an ∼3.5 nm diameter have only 18 chains of cellulose,[2,54] and about 44% of OH groups of cellulose are exposed at the CMF surface. The surface-exposed OH groups are readily converted to OD groups upon contact with D_2O, which was used for hydration in SFG experiments (Figure S9A). Another ∼44% of OH groups are separated from the surrounding D_2O by only one glucose unit. If cellulose crystallinity is low or the thermal stability of the surface glucan chain is not sufficiently high (as suggested by the larger (200) spacing in XRD than the unit cell dimension of highly-crystalline cellulose Iβ[41]), these interior OH groups of the surface chains can also be changed to OD groups. Then, only ∼11% of total OH groups of 18-chain CMFs would remain intact, which may explain the weakness of the OH SFG signal from CMFs in the face region.

Extending this argument, the high OH intensity in the edge region but negligible in the face region could be explained by CMF bundling. Aligned polymer molecules can crystallize more easily than disordered molecules through interchain binding.[55] The same could pertain to CMFs. The singleton microfibrils can tightly bundle laterally through $(1\bar{1}0)$ or (110) facets via hydrogen-bonding interactions and (200) facets via van der Waals interactions. As CMFs bundle together, the fraction of the interior OH groups that cannot be converted to OD groups by D_2O increases (Figure S9B), and these interior OH groups can generate strong OH signals in SFG measurements of cell walls

https://doi.org/10.1021/acs.biomac.3c00538
Biomacromolecules 2023, 24, 4759–4770

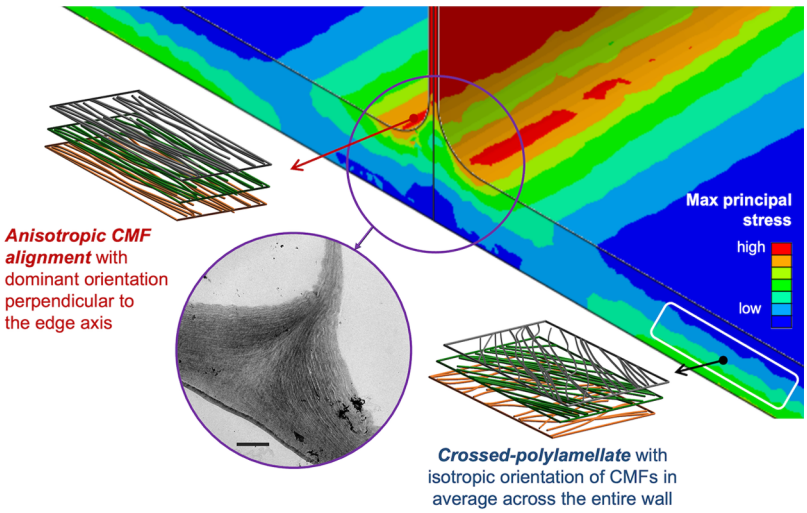

Figure 7. Nonuniform stress distribution and cellulose microfibril assemblies in the epidermis. FEA simulation result shows the maximum principal stress in a rectangular prism under pressure inside. The details are in Figure S10. The schematic drawings show the cellulose microfibril orientational distributions in the edge and face regions of the outermost periclinal walls. The TEM image is the edge region of the cross-sectioned fifth-scale onion epidermis (scale bar = 2 μm). A similar trend was observed in three replicates (Figure S7M−O).

hydrated with D_2O.[56,57] Thus, it could be inferred that CMFs packed along the preferential orientation direction in the edge region may be more highly bundled laterally than is the case for CMFs in the face region. Furthermore, the SFG spectral features in the edge region are consistent with those of tension wood and ramie fibers in which CMFs are highly aligned and bundled.[44,51]

Regiospecific Variation in CMF Assembly and Nonuniform Stress Distribution. Combining all information obtained from SFG microscopy, CP-transmission microscopy, and FESEM analyses, a comprehensive model describing the CMF arrangement in the outermost epidermal walls is constructed as Figure 7. The face region has the crossed-polylamellate structure as documented previously.[18,22] On the other hand, in the edge region, CMFs are preferentially aligned perpendicular to the anticlinal plane and likely to be bundled more than those in the face region. Analysis of cross-sectioned samples by transmission electron microscopy (TEM) (inset of Figure 7) confirms that lamellae in the edge region, except for a small portion near the cuticle side, gradually tilt away from the periclinal plane and transition toward the anticlinal plane. The anticlinal walls of the epidermis are much thinner than the periclinal walls. Thus, it is likely that not all CMF-containing lamellae of the periclinal wall are continuously connected to those of the anticlinal wall.

Then, an important question arises—why are CMFs in the edge region preferentially aligned perpendicular to the edge? One possible hypothesis is that the anisotropic orientation is caused by mechanical stress caused by turgor pressure in the epidermal cell corner. It has been reported that the microtubule alignment, and hence the direction of the CMF deposition, correlates with the maximum tensile stress direction.[34,58] To assess the direction of wall stress in the epidermal cell wall studied here, FEA was conducted with a simple rectangular prism cell model mimicking the epidermal cells. In this model, five facets with thin walls were assumed to be confined by neighboring cells, while the bottom side with a thick periclinal wall was allowed to deform. A load was applied to the inner walls mimicking the turgor pressure inside cells. The FEA result indeed predicted that the stress in the edge is higher than the face region, and the maximal stress direction in the edges is perpendicular to the edge lines as shown in Figure S10B. This supports the hypothesis that, due to the rectangular cross-sectional geometry, the turgor pressure of the cell causes a higher tensile stress in the edge region, which could be the reason or mechanism that CMFs are deposited anisotropically with their preferential axis perpendicular to the anticlinal wall plane.[34,36,58]

The subcellular-level regio-specificity of the CMF deposition pattern sheds light on the discrepancy between microscale imaging of the face region with AFM and FESEM and macroscale spectroscopic studies of epidermal peels. In the previous SFG analyses of large-area samples encompassing walls of multiple cells, the average orientation of CMFs was considered to be transversely biased; but this can be attributed to the sampling bias.[16] Due to the elongated cell shape, the longitudinal edge fraction is larger than the transverse edge fraction in a given area. In other words, transversely aligned CMFs in the longitudinal edge region are sampled more in the large probe area analysis. This sampling bias effect can be seen in the SFG spectra of the whole area (black in Figure 3E,F), which are the average of the entire scanned area.

The preferentially aligned CMFs in the edge region may also contribute to the anisotropic extensibility of onion epidermal peels with nearly isotropic or diagonally distributed CMF orientations. A polarized-IR microscopy study of a second-scale onion epidermis found that the average orientation angle of CMFs in the face region is ~54° with respect to the longitudinal cell axis, which could be interpreted as random (since the value is close to the 54.7° magic angle) or slightly preferentially oriented toward the transverse direction (since the value is larger than 45°).[25] In the previous study, it was argued that CMFs in the face region would be likely to be tilted more toward the transverse direction based on the observation that, under a tensile stress of ~4 MPa, the second-scale abaxial epidermis of onion was stretched by ~13% in the longitudinal direction but only 11% in the transverse direction.[25] However, the microscopic SFG (Figure 3) and CP-transmission (Figure 5) data of this study indicate that CMF orientations across the entire wall thickness of the face region are consistent with nearly isotropic or diagonally bimodal distribution.[24] Then, the 54° angle found in the polarized-IR microscopy analysis should be interpreted as

https://doi.org/10.1021/acs.biomac.3c00538
Biomacromolecules 2023, 24, 4759−4770

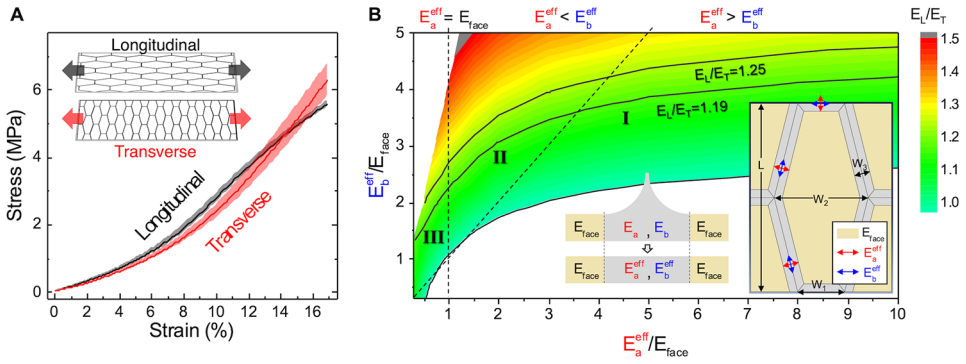

Figure 8. Anisotropic nonlinear stress−strain behavior of onion epidermis. (A) Stress−strain curve from uniaxial tensile tests of the abaxial wall of the fifth-scale onion in the longitudinal and transverse directions. (B) Isoline map of the calculated E_L/E_T ratio as a function of E_a^{eff}/E_{face} and E_b^{eff}/E_{face} for an elastic (small) strain along the longitudinal and transverse directions. Insets show how effective modulus along the direction perpendicular and parallel to the intercellular edge line (E_a^{eff} and E_b^{eff}) is defined and the cell-scale RVE model. The longitudinal and transverse dimensions of the individual cell (L = 120 μm, W_1 = 30 μm, W_2 = 60 μm, W_3 = 10 μm) were adapted from the previous FEA study by Shafayet Zamil et al.[39] The solid isolines are marked at E_L/E_T = 1.0, 1.19 (the calculated value from A) and 1.25 (study by Shafayet Zamil et al.[39]).

a case of equal probability of all possible orientations. If so, the anisotropic extensibility may originate from the anisotropic alignment of CMFs in the edge region (Figure 7).[25] When the preferentially aligned CMF organization in the edge is included, the fraction of the more extensible cell wall, in which CMFs are aligned perpendicular to the stretch direction, is larger when stretched in the longitudinal direction than in the transverse direction due to the elongated cell shape.

Possible Correlation with Anisotropy in the Tissue-Level Modulus. To study the implication of the regiospecific CMF assemblies in the edge region and anisotropic cell shapes on the tissue-level anisotropic mechanical properties of primary cell walls, we employed the onion epidermis for mechanical testings. The stress−strain curves of onion-scale epidermal cell walls show, in general, a relatively linear stress response in a small strain followed by a strain stiffening and yielding behavior at larger strains,[5,39,59] even though there are some variances due to differences in sample preparation, tissue thickness, and clamping method. The fifth-scale abaxial epidermis of onion also shows the same nonlinear behavior (Figure 8A). It is interesting to note that the modulus appears to be higher along the longitudinal direction at a small strain (<6%) but larger along the transverse direction at a large strain (>12%). This suggests more significant strain stiffening along the transverse direction.[12]

In Figure 8A, in the small strain regime (0−3%), the calculated elastic modulus was 15.3 ± 4.0 MPa in the longitudinal direction (E_L) and 12.9 ± 1.2 MPa in the transverse direction (E_T), giving an E_L/E_T ratio of ∼1.2. This trend is in qualitative agreement with the previous literature.[39] Even though the species or tissues are different, several other studies with plant epidermis have reported that the elastic modulus in the small strain is larger in the longitudinal direction.[37,38,60] Such tissue-level anisotropy is difficult to explain if the entire cell wall has a uniform CMF structure.[39,60] Thus, some studies have suggested the net anisotropic orientation of CMFs within the periclinal cell wall,[25,60] which is possible if the distribution of CMFs in the crossed-polylamellate structure or diagonally bimodal distribution in the periclinal wall is slightly skewed into one direction. As an additional factor or alternative explanation, the anisotropic alignment of CMFs in the edge region (Figure 7) could contribute to the tissue-level anisotropy.

To estimate the potential impact of the anisotropic alignment of CMFs in the edge region on the tissue-level anisotropy of tensile modulus in the small strain region, FEA was conducted with an elastic model. The anisotropic elastic modulus of the edge region in which thickness varies gradually is difficult to incorporate into our simple model; thus, the effects of modulus and thickness changes are lumped into a single effective modulus, which simplifies the peeled epidermis model into a two-dimensional structure (see the inset of Figure 8B). Since CMFs are aligned anisotropically in the edge region (Figure 7), the effective modulus in the direction perpendicular to the edge (E_a^{eff}) was allowed to vary independently from that in the direction parallel to the edge (E_b^{eff}). Then, FEA calculated the possible E_a^{eff}/E_{face} and E_b^{eff}/E_{face} solutions for given E_L/E_T ratios for elastic strain along the longitudinal and transverse directions (Figure 8B).

Here, the most plausible solution is the area where $E_a^{eff} > E_b^{eff}$ (region-I, right side of the diagonal dotted line in Figure 8B). Assuming CMFs are the major load-bearing component,[5] the E_a^{eff} along the preferential alignment direction of CMFs is expected to be larger than the E_b^{eff} perpendicular to the CMF alignment direction. In this case, the edge region modulus (E_a^{eff}, E_b^{eff}) should also be larger than the face region modulus (E_{face}). This is consistent with the higher SFG intensity in the edge region than in the face region, which suggests more crystalline CMFs or a higher degree of CMF bundling as mentioned above.

The solution with $E_{face} < E_a^{eff} < E_b^{eff}$ (region-II in Figure 8B) is mathematically possible but physically inconceivable because the elastic modulus of cell walls in which microfibrils are along the stretch direction (E_a^{eff}) is expected to be higher than that of cell walls in which microfibrils are perpendicular to the stretch direction (E_b^{eff}).[5] When cell walls are stretched in the direction perpendicular to the microfibrils, microfibrils are separated and curved, carrying a little load.[5] If CMFs are not the main load-bearing component in the edge region because of the deviation of the lamella plane from the tensile stress axis (see the TEM image in Figure 7), then E_a^{eff} could be smaller than E_{face} (region-III in Figure 8B). This would be the case where compression or shear of the pectin-rich region between adjacent lamellae is the main strain response under small stress.

When CMFs are the main load-bearing component,[5] as in the case of large strains, the stretch along the preferential alignment direction of CMFs would be more difficult than that in the orthogonal direction. Due to the anisotropic shape of the cell, there are more longitudinal edges than transverse edges in a

https://doi.org/10.1021/acs.biomac.3c00538
Biomacromolecules 2023, 24, 4759−4770

given square-shaped area (Figure 3D). Thus, there is a larger fraction of CMFs that are aligned along the transverse direction than the longitudinal direction. This may explain why the strain at the large stress is smaller along the transverse direction (Figure 8A).[25] Thus, the anisotropic CMF orientations in the edge region could be the main reason that the strain stiffening behavior is more prominent along the transverse direction,[12] leading to a crossover from $E_L > E_T$ in the small strain regime to $E_L < E_T$ in the large strain regime.

CONCLUSIONS

Microscopic SFG analysis, which can selectively detect cellulose in cell walls without interferences from other matrix components, was used for subcellular imaging of epidermal walls of *Arabidopsis* stem, maize coleoptile, and onion scales. In the single cell wall epidermal peels, CMFs were found to be preferentially aligned perpendicular to the anticlinal wall plane in the edge region where two cells meet, which is distinct from the isotropic alignment of CMFs in the face region. This finding was corroborated by the CP-transmission microscopy and FESEM analysis of the onion epidermis. The preferential alignment of CMFs in the edge region coincides with the tensile stress directions in the nonuniform stress distribution around a square prism mimicking epidermal cells as determined through FEA. Besides the aligned microfibrils, the assembly in the edge region is also distinct from that in the face region in that it has high SFG intensities, which suggest microfibril bundling. This discovery resolved discrepancies in previous microfibril structure studies obtained by different techniques. The FEA of tensile extension of onion epidermal peels with the nonuniform CMF assemblies suggests that the edge region may contribute to the anisotropy in the tensile mechanical properties of the epidermis.

ASSOCIATED CONTENT

Supporting Information

The Supporting Information is available free of charge at https://pubs.acs.org/doi/10.1021/acs.biomac.3c00538.

Replicates of the microscopic SFG analysis of the epidermal peels, microscopic SFG analysis of cross-sectioned onion epidermis, optical and cross-polarization micrographs of an onion epidermal peel with ruptured anticlinal walls, details of cross-polarization intensity calculation, replicates of SEM and TEM images, microfibril orientation analysis in the SEM image, the count of surface and interior OH groups in bundled cellulose microfibrils, and nonuniform stress distribution in a prism through FEA (PDF)

AUTHOR INFORMATION

Corresponding Author

Seong H. Kim − *Department of Chemical Engineering and Materials Research Institute, Pennsylvania State University, University Park, Pennsylvania 16802, United States;* orcid.org/0000-0002-8575-7269; Email: shk10@psu.edu

Authors

Jongcheol Lee − *Department of Chemical Engineering and Materials Research Institute, Pennsylvania State University, University Park, Pennsylvania 16802, United States;* orcid.org/0000-0003-4877-901X

Juseok Choi − *Department of Chemical Engineering and Materials Research Institute, Pennsylvania State University, University Park, Pennsylvania 16802, United States;* orcid.org/0000-0002-0988-6544

Luyi Feng − *Department of Engineering Science and Mechanics and Bioengineering, Materials Research Institute, Pennsylvania State University, University Park, Pennsylvania 16802, United States*

Jingyi Yu − *Department of Biology, Pennsylvania State University, University Park, Pennsylvania 16802, United States*

Yunzhen Zheng − *Department of Biology, Pennsylvania State University, University Park, Pennsylvania 16802, United States*

Qian Zhang − *Department of Biology, Pennsylvania State University, University Park, Pennsylvania 16802, United States*

Yen-Ting Lin − *Department of Chemical Engineering and Materials Research Institute, Pennsylvania State University, University Park, Pennsylvania 16802, United States*

Saroj Sah − *Department of Biochemistry and Molecular Biology, Pennsylvania State University, University Park, Pennsylvania 16802, United States*

Ying Gu − *Department of Biochemistry and Molecular Biology, Pennsylvania State University, University Park, Pennsylvania 16802, United States*

Sulin Zhang − *Department of Engineering Science and Mechanics and Bioengineering, Materials Research Institute, Pennsylvania State University, University Park, Pennsylvania 16802, United States*

Daniel J. Cosgrove − *Department of Biology, Pennsylvania State University, University Park, Pennsylvania 16802, United States*

Complete contact information is available at: https://pubs.acs.org/10.1021/acs.biomac.3c00538

Notes

The authors declare no competing financial interest.

ACKNOWLEDGMENTS

This work was supported as part of the Center for Lignocellulose Structure and Formation, an Energy Frontier Research Center funded by the U.S. Department of Energy, Office of Science, Basic Energy Sciences under award DE-SC0001090. The authors thank Dr. Kabindra Kafle, Prof. Hojae Yi, and Prof. Tuo Wang for their helpful discussion.

REFERENCES

(1) Somerville, C.; Bauer, S.; Brininstool, G.; Facette, M.; Hamann, T.; Milne, J.; Osborne, E.; Paredez, A.; Persson, S.; Raab, T.; et al. Toward a systems approach to understanding plant cell walls. *Science* **2004**, *306*, 2206−2211.

(2) Cosgrove, D. J. Nanoscale structure, mechanics and growth of epidermal cell walls. *Curr. Opin. Plant Biol.* **2018**, *46*, 77−86.

(3) Cosgrove, D. J. Plant cell wall extensibility: connecting plant cell growth with cell wall structure, mechanics, and the action of wall-modifying enzymes. *J. Exp. Bot.* **2016**, *67*, 463−476.

(4) Burton, R. A.; Gidley, M. J.; Fincher, G. B. Heterogeneity in the chemistry, structure and function of plant cell walls. *Nat. Chem. Biol.* **2010**, *6*, 724−732.

(5) Zhang, Y.; Yu, J.; Wang, X.; Durachko, D. M.; Zhang, S.; Cosgrove, D. J. Molecular insights into the complex mechanics of plant epidermal cell walls. *Science* **2021**, *372*, 706−711.

(6) Cosgrove, D. J. Re-constructing our models of cellulose and primary cell wall assembly. *Curr. Opin. Plant Biol.* **2014**, *22*, 122−131.
(7) Purushotham, P.; Ho, R.; Zimmer, J. Architecture of a catalytically active homotrimeric plant cellulose synthase complex. *Science* **2020**, *369*, 1089−1094.
(8) Lee, C. M.; Mohamed, N. M.; Watts, H. D.; Kubicki, J. D.; Kim, S. H. Sum-frequency-generation vibration spectroscopy and density functional theory calculations with dispersion corrections (DFT-D2) for cellulose Ialpha and Ibeta. *J. Phys. Chem. B* **2013**, *117*, 6681−6692.
(9) Makarem, M.; Lee, C. M.; Kafle, K.; Huang, S.; Chae, I.; Yang, H.; Kubicki, J. D.; Kim, S. H. Probing cellulose structures with vibrational spectroscopy. *Cellulose* **2019**, *26*, 35−79.
(10) Nishiyama, Y.; Langan, P.; Chanzy, H. Crystal Structure and Hydrogen-Bonding System in Cellulose Iβ from Synchrotron X-ray and Neutron Fiber Diffraction. *J. Am. Chem. Soc.* **2002**, *124*, 9074−9082.
(11) Cosgrove, D. J.; Jarvis, M. C. Comparative structure and biomechanics of plant primary and secondary cell walls. *Front. Plant Sci.* **2012**, *3*, 204.
(12) Bidhendi, A. J.; Geitmann, A. Relating the mechanics of the primary plant cell wall to morphogenesis. *J. Exp. Bot.* **2016**, *67*, 449−461.
(13) Cosgrove, D. J. Growth of the plant cell wall. *Nat. Rev. Mol. Cell Biol.* **2005**, *6*, 850−861.
(14) Ye, D.; Rongpipi, S.; Kiemle, S. N.; Barnes, W. J.; Chaves, A. M.; Zhu, C.; Norman, V. A.; Liebman-Pelaez, A.; Hexemer, A.; Toney, M. F.; et al. Preferred crystallographic orientation of cellulose in plant primary cell walls. *Nat. Commun.* **2020**, *11*, No. 4720.
(15) Wilson, R. H.; Smith, A. C.; Kačuráková, M.; Saunders, P. K.; Wellner, N.; Waldron, K. W. The Mechanical Properties and Molecular Dynamics of Plant Cell Wall Polysaccharides Studied by Fourier-Transform Infrared Spectroscopy1. *Plant Physiol.* **2000**, *124*, 397−406.
(16) Kafle, K.; Xi, X.; Lee, C. M.; Tittmann, B. R.; Cosgrove, D. J.; Park, Y. B.; Kim, S. H. Cellulose microfibril orientation in onion (*Allium cepa* L.) epidermis studied by atomic force microscopy (AFM) and vibrational sum frequency generation (SFG) spectroscopy. *Cellulose* **2014**, *21*, 1075−1086.
(17) Suslov, D.; Verbelen, J. P.; Vissenberg, K. Onion epidermis as a new model to study the control of growth anisotropy in higher plants. *J. Exp. Bot.* **2009**, *60*, 4175−4187.
(18) Zhang, T.; Zheng, Y.; Cosgrove, D. J. Spatial organization of cellulose microfibrils and matrix polysaccharides in primary plant cell walls as imaged by multichannel atomic force microscopy. *Plant J.* **2016**, *85*, 179−192.
(19) Zhang, T.; Cosgrove, D. Preparation of Onion Epidermal Cell Walls for Imaging by Atomic Force Microscopy (AFM). *Bio-Protoc.* **2017**, *7*, No. e2647.
(20) Durachko, D.; Park, Y. B.; Zhang, T.; Cosgrove, D. Biomechanical Characterization of Onion Epidermal Cell Walls. *Bio-Protoc.* **2017**, *7*, No. e2662.
(21) Zhang, T.; Mahgsoudy-Louyeh, S.; Tittmann, B.; Cosgrove, D. J. Visualization of the nanoscale pattern of recently-deposited cellulose microfibrils and matrix materials in never-dried primary walls of the onion epidermis. *Cellulose* **2014**, *21*, 853−862.
(22) Zhang, T.; Vavylonis, D.; Durachko, D. M.; Cosgrove, D. J. Nanoscale movements of cellulose microfibrils in primary cell walls. *Nat. Plants* **2017**, *3*, 17056.
(23) Ye, D.; Kiemle, S. N.; Rongpipi, S.; Wang, X.; Wang, C.; Cosgrove, D. J.; Gomez, E. W.; Gomez, E. D. Resonant soft X-ray scattering reveals cellulose microfibril spacing in plant primary cell walls. *Sci. Rep.* **2018**, *8*, No. 12449.
(24) Nicolas, W. J.; Fäßler, F.; Dutka, P.; Schur, F. K. M.; Jensen, G.; Meyerowitz, E. Cryo-electron tomography of the onion cell wall shows bimodally oriented cellulose fibers and reticulated homogalacturonan networks. *Curr. Biol.* **2022**, *32*, 2375−2389.e2376.
(25) Kafle, K.; Park, Y. B.; Lee, C. M.; Stapleton, J. J.; Kiemle, S. N.; Cosgrove, D. J.; Kim, S. H. Effects of mechanical stretching on average orientation of cellulose and pectin in onion epidermis cell wall: A polarized FT-IR study. *Cellulose* **2017**, *24*, 3145−3154.
(26) Baskin, T. I.; Beemster, G. T.; Judy-March, J. E.; Marga, F. Disorganization of cortical microtubules stimulates tangential expansion and reduces the uniformity of cellulose microfibril alignment among cells in the root of Arabidopsis. *Plant Physiol.* **2004**, *135*, 2279−2290.
(27) Baskin, T. I. Anisotropic expansion of the plant cell wall. *Annu. Rev. Cell Dev. Biol.* **2005**, *21*, 203−222.
(28) Suslov, D.; Verbelen, J. P. Cellulose orientation determines mechanical anisotropy in onion epidermis cell walls. *J. Exp. Bot.* **2006**, *57*, 2183−2192.
(29) Makarem, M.; Nishiyama, Y.; Xin, X.; Durachko, D. M.; Gu, Y.; Cosgrove, D. J.; Kim, S. H. Distinguishing Mesoscale Polar Order (Unidirectional vs Bidirectional) of Cellulose Microfibrils in Plant Cell Walls Using Sum Frequency Generation Spectroscopy. *J. Phys. Chem. B* **2020**, *124*, 8071−8081.
(30) Lee, C. M.; Kafle, K.; Park, Y. B.; Kim, S. H. Probing crystal structure and mesoscale assembly of cellulose microfibrils in plant cell walls, tunicate tests, and bacterial films using vibrational sum frequency generation (SFG) spectroscopy. *Phys. Chem. Chem. Phys.* **2014**, *16*, 10844−10853.
(31) Barnette, A. L.; Lee, C.; Bradley, L. C.; Schreiner, E. P.; Park, Y. B.; Shin, H.; Cosgrove, D. J.; Park, S.; Kim, S. H. Quantification of crystalline cellulose in lignocellulosic biomass using sum frequency generation (SFG) vibration spectroscopy and comparison with other analytical methods. *Carbohydr. Polym.* **2012**, *89*, 802−809.
(32) Jarvis, M. C.; Briggs, S. P. H.; Knox, J. P. Intercellular adhesion and cell separation in plants. *Plant, Cell Environ.* **2003**, *26*, 977−989.
(33) Elliott, L.; Kirchhelle, C. The importance of being edgy: cell geometric edges as an emerging polar domain in plant cells. *J. Microsc* **2020**, *278*, 123−131.
(34) Hamant, O.; Inoue, D.; Bouchez, D.; Dumais, J.; Mjolsness, E. Are microtubules tension sensors? *Nat. Commun.* **2019**, *10*, No. 2360.
(35) Hamant, O.; Heisler, M. G.; Jönsson, H.; Krupinski, P.; Uyttewaal, M.; Bokov, P.; Corson, F.; Sahlin, P.; Boudaoud, A.; Meyerowitz, E. M.; et al. Developmental patterning by mechanical signals in Arabidopsis. *Science* **2008**, *322*, 1650−1655.
(36) Uyttewaal, M.; Burian, A.; Alim, K.; Landrein, B.; Borowska-Wykręt, D.; Dedieu, A.; Peaucelle, A.; Ludynia, M.; Traas, J.; Boudaoud, A.; et al. Mechanical Stress Acts via Katanin to Amplify Differences in Growth Rate between Adjacent Cells in Arabidopsis. *Cell* **2012**, *149*, 439−451.
(37) Vanstreels, E.; Alamar, M. C.; Verlinden, B. E.; Enninghorst, A.; Loodts, J. K. A.; Tijskens, E.; Ramon, H.; Nicolaï, B. M. Micromechanical behaviour of onion epidermal tissue. *Postharvest Biol. Technol.* **2005**, *37*, 163−173.
(38) Bidhendi, A. J.; Li, H.; Geitmann, A. Modeling the nonlinear elastic behavior of plant epidermis. *Botany* **2020**, *98*, 49−64.
(39) Shafayet Zamil, M.; Yi, H.; Puri, V. M. A multiscale FEA framework for bridging cell-wall to tissue-scale mechanical properties: the contributions of middle lamella interface and cell shape. *J. Mater. Sci.* **2017**, *52*, 7947−7968.
(40) Zhu, X.; Li, S.; Pan, S.; Xin, X.; Gu, Y. CSI1, PATROL1, and exocyst complex cooperate in delivery of cellulose synthase complexes to the plasma membrane. *Proc. Natl. Acad. Sci. U.S.A.* **2018**, *115*, E3578−E3587.
(41) Huang, S.; Makarem, M.; Kiemle, S. N.; Zheng, Y.; He, X.; Ye, D.; Gomez, E. W.; Gomez, E. D.; Cosgrove, D. J.; Kim, S. H. Dehydration-induced physical strains of cellulose microfibrils in plant cell walls. *Carbohydr. Polym.* **2018**, *197*, 337−348.
(42) Huang, S.; Makarem, M.; Kiemle, S. N.; Hamedi, H.; Sau, M.; Cosgrove, D. J.; Kim, S. H. Inhomogeneity of Cellulose Microfibril Assembly in Plant Cell Walls Revealed with Sum Frequency Generation Microscopy. *J. Phys. Chem. B* **2018**, *122*, 5006−5019.
(43) Lee, C. M.; Kafle, K.; Huang, S.; Kim, S. H. Multimodal Broadband Vibrational Sum Frequency Generation (MM-BB-V-SFG) Spectrometer and Microscope. *J. Phys. Chem. B* **2016**, *120*, 102−116.
(44) Choi, J.; Lee, J.; Makarem, M.; Huang, S.; Kim, S. H. Numerical Simulation of Vibrational Sum Frequency Generation Intensity for Non-Centrosymmetric Domains Interspersed in an Amorphous

https://doi.org/10.1021/acs.biomac.3c00538
Biomacromolecules 2023, 24, 4759−4770

Matrix: A Case Study for Cellulose in Plant Cell Wall. *J. Phys. Chem. B* **2022**, *126*, 6629−6641.
(45) Zheng, Y.; Cosgrove, D. J.; Ning, G. High-Resolution Field Emission Scanning Electron Microscopy (FESEM) Imaging of Cellulose Microfibril Organization in Plant Primary Cell Walls. *Microsc. Microanal.* **2017**, *23*, 1048−1054.
(46) Püspöki, Z.; Storath, M.; Sage, D.; Unser, M. Transforms and Operators for Directional Bioimage Analysis: A Survey. In *Focus on Bio-Image Informatics*; De Vos, W. H.; Munck, S.; Timmermans, J.-P., Eds.; Springer: Cham, 2016; Vol. *219*; pp 69−93.
(47) Xi, X.; Kim, S. H.; Tittmann, B. Atomic force microscopy based nanoindentation study of onion abaxial epidermis walls in aqueous environment. *J. Appl. Phys.* **2015**, *117*, No. 024703.
(48) Cosgrove, D. J. Tansley Review No. 46. Wall Extensibility: Its Nature, Measurement and Relationship to Plant Cell Growth. *New Phytol.* **1993**, *124*, 1−23.
(49) Beauzamy, L.; Derr, J.; Boudaoud, A. Quantifying hydrostatic pressure in plant cells by using indentation with an atomic force microscope. *Biophys. J.* **2015**, *108*, 2448−2456.
(50) Omairey, S. L.; Dunning, P. D.; Sriramula, S. Development of an ABAQUS plugin tool for periodic RVE homogenisation. *Eng. Comput.* **2019**, *35*, 567−577.
(51) Kafle, K.; Shi, R.; Lee, C. M.; Mittal, A.; Park, Y. B.; Sun, Y.-H.; Park, S.; Chiang, V.; Kim, S. H. Vibrational sum-frequency-generation (SFG) spectroscopy study of the structural assembly of cellulose microfibrils in reaction woods. *Cellulose* **2014**, *21*, 2219−2231.
(52) Lee, J.; Chaves, A. M.; Choi, J.; Roberts, A. W.; Kim, S. H. Sum frequency generation (SFG) microscopy analysis of cellulose microfibrils in Physcomitrium patens gametophore leaf. *Cellulose* **2023**, No. 05355.
(53) Chen, X.; Lee, C. M.; Wang, H.-F.; Jensen, L.; Kim, S. H. Experimental and Theoretical Study of Azimuth Angle and Polarization Dependences of Sum-Frequency-Generation Vibrational Spectral Features of Uniaxially Aligned Cellulose Crystals. *J. Phys. Chem. C* **2017**, *121*, 18876−18886.
(54) Kubicki, J. D.; Yang, H.; Sawada, D.; O'Neill, H.; Oehme, D.; Cosgrove, D. The Shape of Native Plant Cellulose Microfibrils. *Sci. Rep.* **2018**, *8*, No. 13983.
(55) Nitta, K.-h. On the Orientation-Induced Crystallization of Polymers. *Polymers* **2016**, *8*, 229.
(56) Hofstetter, K.; Hinterstoisser, B.; Salmén, L. Moisture uptake in native cellulose—the roles of different hydrogen bonds: a dynamic FT-IR study using Deuterium exchange. *Cellulose* **2006**, *13*, 131−145.
(57) Huang, S.; Kiemle, S. N.; Makarem, M.; Kim, S. H. Correlation between crystalline cellulose structure and cellulose synthase complex shape: a spectroscopic study with unicellular freshwater alga Micrasterias. *Cellulose* **2020**, *27*, 57−69.
(58) Zhao, F.; Du, F.; Oliveri, H.; Zhou, L.; Ali, O.; Chen, W.; Feng, S.; Wang, Q.; Lü, S.; Long, M.; et al. Microtubule-Mediated Wall Anisotropy Contributes to Leaf Blade Flattening. *Curr. Biol.* **2020**, *30*, 3972−3985.e3976.
(59) Pieczywek, P. M.; Zdunek, A. Finite element modelling of the mechanical behaviour of onion epidermis with incorporation of nonlinear properties of cell walls and real tissue geometry. *J. Food Eng.* **2014**, *123*, 50−59.
(60) Majda, M.; Trozzi, N.; Mosca, G.; Smith, R. S. How Cell Geometry and Cellular Patterning Influence Tissue Stiffness. *Int. J. Mol. Sci.* **2022**, *23*, 5651.

https://doi.org/10.1021/acs.biomac.3c00538
Biomacromolecules 2023, 24, 4759−4770